Change in ocean carbon sequestration during ice retreat in the Arctic

Computational Marine Ecological Modelling – 25314

Technical University of Denmark – May 17th, 2023

Giacomo Gardella (s223165), Markus Strange (s194445) & Emil Bohr (s190712)

Table of Contents

Introduction & Background

Global warming has in recent years gained the public attention that climate scientists have strived for, for decades. However, changes in the climate are now occurring rapidly and might take centuries to reverse. The strongest manifestation of climate change is a global temperature rise, which according to the IPCC, is approximately 1.09°C (0.95-1.20) since preindustrial time (IPCC, 2021). Climate change in general and temperature change in specific do not distribute evenly around the globe (Smith et al., 2019). Due to a phenomenon termed “poleward amplification”, warming has been 2 or 3 times higher at the poles compared to lower latitudes (Francis & Wu 2020; Im et al., 2021). In fact, the average annual air temperature in the Arctic region has risen by 2.7°C over the last 5 decades (Box et al. 2019). One of the consequences of increasing temperature in the Arctic is loss of sea ice. Over the last 5 decades, the area of Arctic sea ice has declined by 40% (Box et al., 2019). Future projections are even more worrying. Under a +2°C end-of-century warming scenario, the probability of having an ice-free Arctic Ocean during the month of September before 2100 is 100% (Jahn, 2018). As the ecosystem in the Arctic region is highly adapted to abundance of sea ice (Lannuzel et.al., 2020), a disappearance of sea ice might alter the ecosystem, and push it towards a more classical temperate one, where the spring bloom is initiated by solar direct radiation, rather than the current break of the ice. This change in the Arctic could also mean changes in the services performed by the ecosystem for the benefit of humankind. The main services of the Arctic ecosystem, both historically and present, are production of food and sequestration of carbon, which has a buffering effect on climate change. Sequestration of carbon by biological processes (the biological pump) is important for global climate regulation, and therefore quantification both on local and global scale, would give a better understanding of possible opportunities and tipping points for the future. Mathematical modelling is a widely recognised discipline for general patterns and projections in ecology. Among the published mathematicel models, the so-called Fasham model (Fasham et al.,1990) is useful for understanding trends in a simplified planktonic food web.

In the present study, we apply a slightly modified version of Fasham et al.’s model from 1990 and adjust the parameters for an Arctic ecosystem (at 70° N). The aim of our study is to answer the question:

How much carbon sinks into the sediment and thereby is sequestered under different scenarios of sea ice cover in the Arctic Ocean?

Our model considers phytoplankton, zooplankton, detritus, bacteria, and various forms of dissolved nitrogen. Our baseline climate scenario is six months of sea ice, and then we investigate climate scenarios of four and two months of ice.

In our study we found that carbon sequestration will slightly decrease if the duration of sea ice is reduced, however production of zooplankton would increase substantially, which provide more food for higher trophic levels, and potentially a higher fisheries yield.

Conceptual model

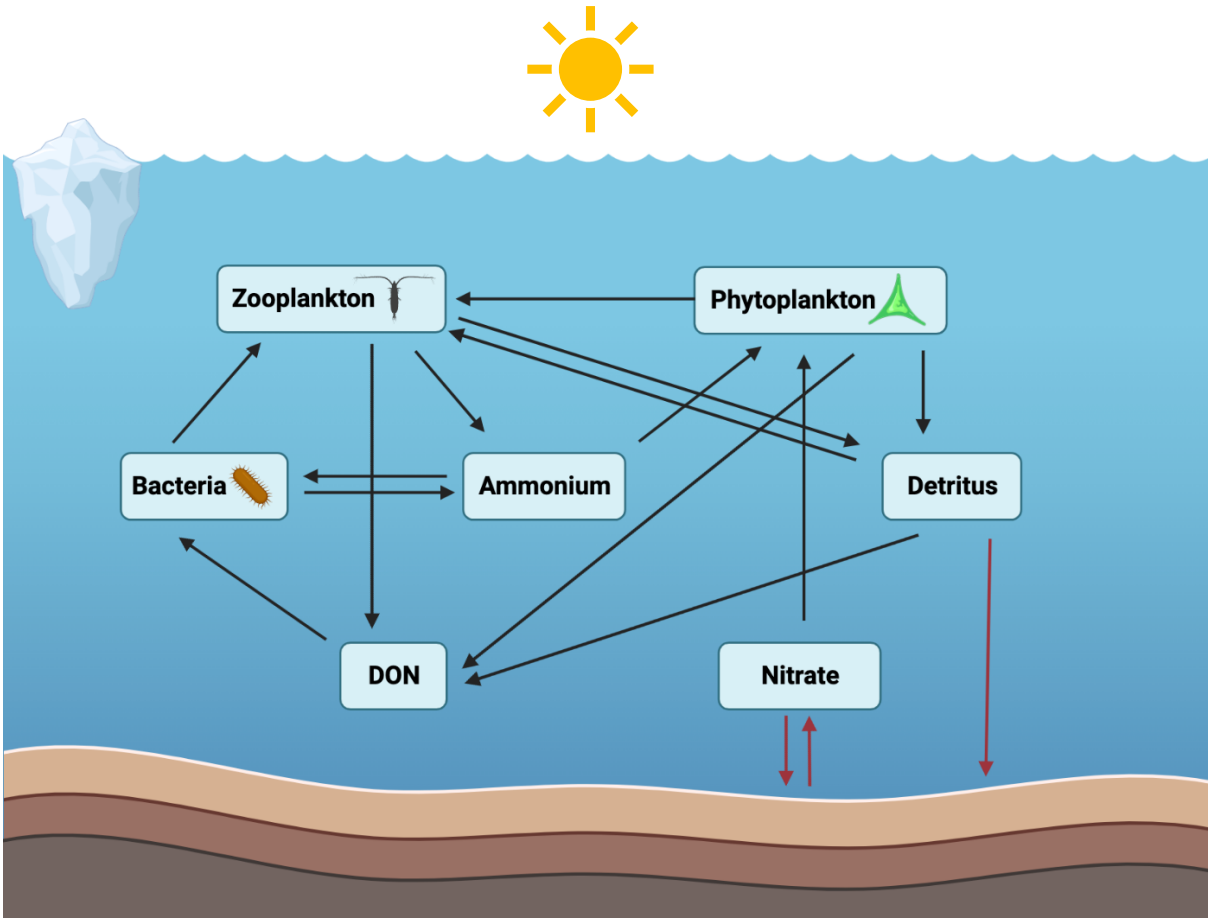

Figure 1: Schematic of the model used in this study. DON is dissolved organic nitrogen.

Figure 1 shows the schematics of our simplified Arctic ecosystem. Primary production is performed by phytoplankton, that take up nitrogen as either ammonium or nitrate. Phytoplankton either dies off as detritus, is grazed upon by zooplankton or leaches DON. Zooplankton graze on both phytoplankton, bacteria, and detritus. Zooplankton either contribute to the dissolved nutrients by sloppy feeding (DON) and excretion (ammonium) or to the detritus by fecal pellets. Bacteria play the role of reparticulation of nutrients by DON and ammonium uptake and of remineralization by ammonium excretion. The only exchange of nutrients with the outside of our system is by detritus sinking to the bottom (sequestration) and diffusion of nitrate between the sediment and bottom water.

As our system is a very simplified proxy of an Arctic ecosystem, there are some features, which we do not catch and therefore our model does not completely reflect the nature. One of these is the microbial community, where we only have heterotrophic bacteria. In nature, the bacterial community play a crucial role in the nitrogen cycle, as they can both fix atmospheric

nitrogen (nitrogen fixation), turn fixed nitrogen into atmospheric nitrogen (denitrification), and turn ammonium into nitrate (nitrification). These processes would all alter our food web, as nitrogen fixation and denitrification would give nitrogen influx and outflux to our system, respectively, and nitrification would turn our deep-sea ammonium into nitrate (see Figure 5). Another simplification in our system is that we have a constant mortality of zooplankton (i.e., no higher trophic levels). This probably changes the temporal and spatial dynamics of our food web, especially seen in the very high autumn abundance of zooplankton (see Figure 6), but overall, we do not expect it to alter the qualitative patterns.

The final major simplification in our system is that we do not include stratification. In an Arctic environment stratification would occur after the ice breaks both due to freshwater from ice melting and solar radiation. According to Sverdrup's *critical depth hypothesis* (Sverdrup, 1953), the spring bloom will not occur in the absence of an upper mixed layer. We accounted for this by increasing the diffusivity (from Zhang et al., 2007) by a factor of two, which was enough to sustain the whole community. The fact that this was even possible might be evidence against Sverdrup's hypothesis, and rather support the *dilution-recoupling hypothesis* (Behrenfeld, 2010).

As seen from Figure 5 and 6 all state variables are expressed in units of mmol N m^{-3} d^{-1}. This makes the equations simpler and also allow for easier comparisons between state variables. However, for our main results the nitrogen content is converted into carbon either using the Redfield ratio C:N of 106:16 (at the top 200m), or deep sea ratio from Sarmiento et al., (1994) C:N of 117:16 (at the bottom).

Model equations

Phytoplankton

The differential equation describing the change in phytoplankton biomass is defined as follows:

$$\frac{\partial P}{\partial t} = -\frac{\partial J_P}{\partial z} + (1-\gamma)\sigma P - G_P - m_P P$$

, where σ is the average daily phytoplankton specific growth rate, G_P is a function describing the grazing of zooplankton on phytoplankton, γ is the exudation fraction, and m_P is the phytoplankton mortality rate.

Since phytoplankton growth is limited by light and nutrient availability, σ is calculated as a product of J and Q, which are functions describing the light and nutrient limitation on the phytoplankton growth, respectively:

$$\sigma = JQ$$

Light limitation was implemented with a function dependent on parameter, α, describing the initial slope of the phytoplankton versus irradiance (*P-I*) curve and on the maximum growth rate of the phytoplankton, g_P. This function is slightly different from a type II functional response since it reaches a plateau faster. The function was taken unmodified from Fasham et al. (1990) and is defined as follows:

$$J = \frac{\alpha I g_P}{\sqrt{{g_P}^2 + (\alpha I)^2}}$$

The nutrient limitation function, Q, was created based on a type II functional response or Michaelis-Menten equation and was not modified from Fasham et al. (1990). In this equation, the growth is dependent on a half-saturation term, H_P, which represents the nutrient concentration at which the growth is half of the maximum growth rate, g_P. The half-saturation constants for ammonium and nitrate are expected to be similar and therefore here considered to be equal. Phytoplankton are able to obtain nitrogen both from nitrate, N, and from ammonium, A. However, the preferred source of nitrogen is ammonium. Therefore, the presence of ammonium is expected to inhibit the uptake of nitrate, and this effect should be dependent on the concentration of nitrate with an exponential coefficient ψ. The resulting nutrient limitation used is (Fasham et al., 1990):

$$Q = Q_1 + Q_2 = \frac{N e^{-\psi A}}{H_P + N} + \frac{A}{H_P + A}$$

Zooplankton

The zooplankton population grows by grazing on bacteria, phytoplankton, and detritus. These consumptions are implemented with grazing functions, G_B, G_P, and G_D, respectively, multiplied by an assimilation efficiency, β. Losses of zooplankton are caused by a mortality rate, m_Z, and by a loss of dissolved nitrogen through excretion, described by the excretion rate μ_Z. All effects are combined in the following differential equation:

$$\frac{\partial Z}{\partial t} = -\frac{\partial J_Z}{\partial z} + \beta G_P + \beta G_B + \beta G_D - m_Z Z - \mu_Z Z$$

Since zooplankton graze on bacteria, detritus, and phytoplankton, a function describing the total food availability, *food*, can be created, by adding the concentration of the three prey items, each multiplied by a corresponding preference factor:

$$food = p_P P + p_B B + p_D D$$

It is expected that zooplankton feed following a type II functional response, since this is the most common functional response observed for multiple zooplankton groups, including copepods. Consequently, a half saturation for the ingestion by zooplankton, H_Z, was defined. This parameter, along with the *food* function, the preferences of zooplankton for prey items, and the maximum growth rate of zooplankton, g_Z, were used to define the grazing functions for phytoplankton, bacteria, and detritus as follows:

$$G_P = g_Z Z \frac{p_P P}{H_Z + food}$$

$$G_B = g_Z Z \frac{p_B B}{H_Z + food}$$

$$G_D = g_Z Z \frac{p_D D}{H_Z + food}$$

Bacteria

Our model only considers heterotrophic bacteria that utilize dissolved organic nitrogen and ammonium. Therefore, the only factors contributing to bacterial growth are dissolved organic nitrogen uptake, described by the function U_1, and ammonia uptake, described by the function U_2. Losses are caused by predation by zooplankton and by losses of ammonium, described by the bacterial excretion rate μ_B. The resulting differential equation is:

$$\frac{\partial B}{\partial t} = -\frac{\partial J_B}{\partial z} + U_1 + U_2 - G_B - \mu_B B$$

While bacteria feed on ammonium and dissolved organic nitrogen, these food sources are not interchangeable (Fasham et al., 1990). Therefore, both nutrients are needed in a ratio η. Bacterial growth will depend on the limiting nutrient between the two, as suggested by Liebig's law of the minimum:

$$S = \text{MIN}(A, \eta DON)$$

Similarly to phytoplankton and zooplankton, it is expected that the bacterial uptake of dissolved organic nitrogen and ammonium follows a type II functional response. Therefore, a half saturation constant for bacteria, H_B, was defined. This was assumed to be equal for both ammonium and dissolved organic nitrogen uptake. Finally, the functions U_1 and U_2 can be defined as follows:

$$U_1 = \frac{g_B B \cdot DON}{H_B + S + DON}$$

$$U_2 = \frac{g_B B S}{H_B + S + DON}$$

Detritus

The net sources of detritus in the system are fecal pellets produced by zooplankton following the ingestion of bacteria and phytoplankton, as well as dead phytoplankton. Grazing of detritus by zooplankton and detrital breakdown by bacteria, defined by the detrital breakdown rate, m_D, represent the losses of detritus. Combined the change of detritus is calculated as:

$$\frac{\partial D}{\partial t} = -\frac{\partial J_D}{\partial z} + (1-\beta)G_P + (1-\beta)G_B - \beta G_D - m_D D + m_P P$$

Nitrate

The only biological process affecting the nitrate concentration in our system is the uptake by phytoplankton, which was described above. In addition, there is an input of nitrate in the system due to the fact that the water at the bottom is in or attempts to reach equilibrium with the nitrate concentration in the sediments. The differential equation for the nitrate is:

$$\frac{\partial N}{\partial t} = -\frac{\partial J_N}{\partial z} - J Q_1 P$$

Ammonium

Ammonium is being released by zooplankton and bacteria through excretion, and through remineralization of zooplankton consumed by predators. Since only a fraction of the compounds excreted by zooplankton is ammonium, the parameter ε accounting for this fraction was defined. The higher trophic levels are not modelled here but are accounted for with a parameter that describes the fraction of dead zooplankton that is not remineralized, Ω. Ammonium is consumed by phytoplankton for the regenerated primary production and by bacteria. The overall change is described by the following equation:

$$\frac{\partial A}{\partial t} = -\frac{\partial J_A}{\partial Z} - JQ_2P - U_2 + \mu_B B + Z\left(\varepsilon\mu_Z + m_Z(1-\Omega)\right)$$

Dissolved organic nitrogen - DON

Sources of dissolved organic nitrogen include exudation by phytoplankton, excretion and sloppy feeding by zooplankton, and breakdown of detritus (Fasham et al., 1990). The only loss is given by the bacterial uptake.

$$\frac{\partial DON}{\partial t} = -\frac{\partial J_{DON}}{\partial z} + \gamma\sigma P + m_D D + (1-\varepsilon)\mu_Z Z - U_1$$

Seasonality and ice scenarios

The amount of light reaching the surface of the water column varies seasonally in the modelled system. It depends on the day of the year, the latitude, and on the ice cover. A cosine function, *season*, was created to account for the effects of day of year and latitude, although the latitude was fixed here to 70°N (Figure 2). The season function was defined as:

$$season = 1 - \left(a - a\cos\left(\frac{\pi\theta}{90}\right)\right)\cos\left(\frac{4\pi}{73} + \frac{2\pi t}{365}\right)$$

$$a = 0.5936313659$$

, where a is a constant, θ is the latitude in °, and t is time in days.

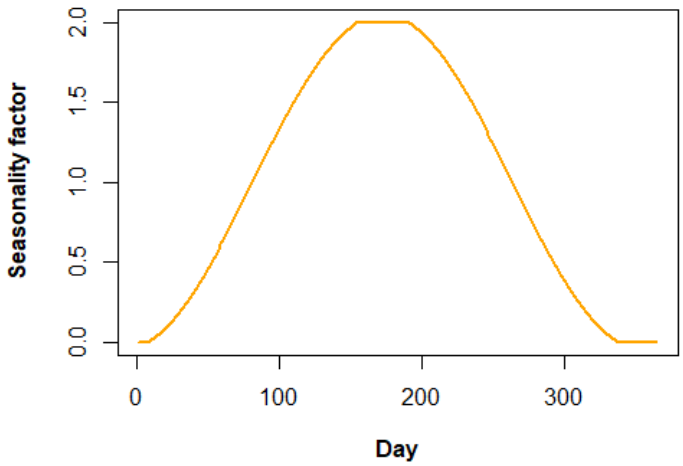

Figure 2: Values of the season function for each day of the year. A value of 0 means no light and a value of 2 means 24 hours of light.

Since the latitude chosen here is above the arctic circle (66.6°N) there is a period of ~35 days in the winter, during which there is no light (Figure 2). Similarly, there is a period of ~35 days in the summer during which there is a maximum light irradiance of 24 hours (Figure 2).

To implement ice cover in the model, a sine function of time, *ice*, was created. The function depends on two parameters, W_{center} and W_{length}, describing, respectively, the center and length of the sea ice cover period. These two parameters were used to derive variables that were combined into the *ice* function as shown below:

$$b = \frac{W_{center} + W_{length}}{2}$$

$$c = \sin\left(\frac{\pi b}{182.5} + \frac{\pi 25}{146}\right)$$

$$d = \frac{1}{\sin\left(\pi \frac{W_{center} - W_{length}}{1095} + \frac{\pi 25}{146}\right) - c}$$

$$ice = -c\,d + d\sin\left(\frac{\pi t}{182.5} + \frac{\pi 25}{146}\right)$$

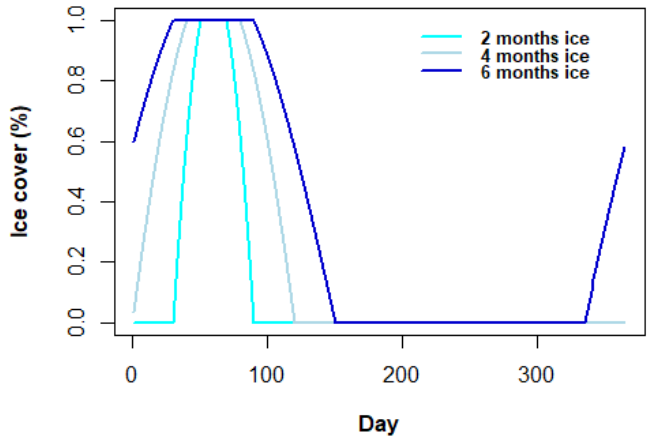

Figure 3: Ice cover, expressed as a fraction of complete ice cover, for each day of the year for all three ice duration scenarios. The baseline conditions are 6 months of ice.

Three scenarios of ice cover were created by changing the W_{length} parameter:

(i) **6 months ice:** 180 days of partial or complete ice cover (baseline)

(ii) **4 months ice:** 120 days of partial or complete ice cover

(iii) **2 months ice:** 60 days of partial or complete ice cover

The function *season* and *ice* were combined to obtain a total seasonal effect on the surface light irradiance:

$$I_s = season \cdot (1 - ice) I_0$$

, where I_s is the light irradiance at the surface for each day of the year.

While the light irradiance at the surface after the 150th day of the year does not change much between the three scenarios, the light availability during the first 150 days of the year changes considerably among the three scenarios (Figure 4).

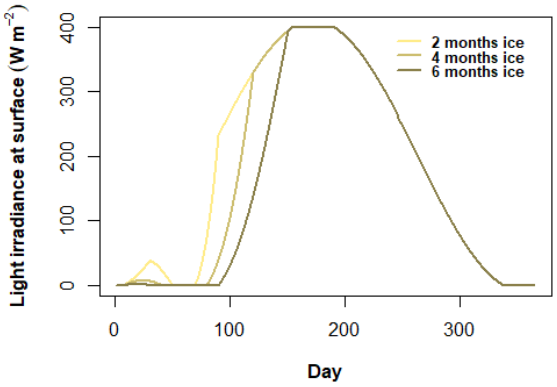

Figure 4. Light irradiance at the surface accounting for the effects of seasonality for the three ice cover scenarios.

In this model, the light availability at each depth needs to be calculated. To do this, accounting for the light absorption by phytoplankton and detritus is crucial. Therefore, a shading coefficient, k_c, for phytoplankton and detritus was defined. On the contrary, the light absorption by bacteria and dissolved substances are not take into account. The light reaching a specific depth is thus affected by the concentration of phytoplankton and detritus in the entire water column above the depth considered. This damping effect can be described by the following equation:

$$damp(t,z) = k_c \Delta z \left(\int_0^z (P(t,\xi) + D(t,\xi)) d\xi \right)$$

, where ξ represents an integration parameter of depth.

Finally, these equations *season*, *ice*, and *damp* are combined with the Lambert-Beer law to derive the light intensity at each depth:

$$I = I_0 \cdot \mathrm{PAR}_0 \cdot \exp\left(-k_w z - damp\right) \cdot season \cdot (1 - ice)$$

, where PAR_0 is the proportion of incoming light radiation that is available for photosynthesis.

Discretization

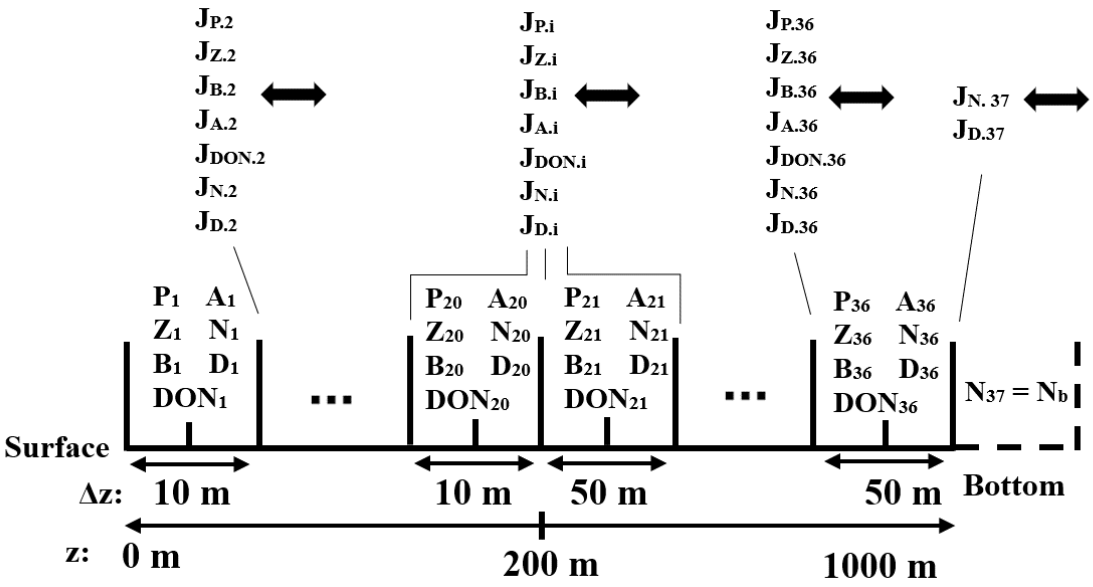

Figure 5: Spatial discretization. In the figure i is 20,21, and 22.

A discretization in space was necessary to solve the model numerically using the software R x64 version 4.2.2 from 31.10.2022 (Copyright (C) 2022 The R Foundation for Statistical Computing). Here, the water column was divided into discrete units, "grid cells". To minimize computational time, the size of the grid cells was set to 10 m for the top 200 m of the water column, and to 50 m for the bottom 800 m of the water column. This allows to obtain a high spatial resolution for the top 200 m, where the most interesting biological patterns can be observed, and a coarser spatial resolution where only broader changes are observed. Since the total depth of the modelled water column is 1000 m, a total of 36 grid cells were created and modelled (Figure 5). The depths at the center of each grid cells were calculated and combined into a vector, z, which was used to describe the water column. The concentrations of all state variables at each value of z were computed as follows:

$$\frac{dP}{dt} = -\frac{J_{P.i+1} - J_{P.i}}{\Delta z} + (1-\gamma)\sigma P - G_P - m_P P$$

$$\frac{dZ}{dt} = -\frac{J_{Z.i+1} - J_{Z.i}}{\Delta z} + \beta G_P + \beta G_B + \beta G_D - m_Z Z - \mu_Z Z$$

$$\frac{dB}{dt} = -\frac{J_{B.i+1} - J_{B.i}}{\Delta z} + U_1 + U_2 - G_B - \mu_B B$$

$$\frac{dD}{dt} = -\frac{J_{D.i+1} - J_{D.i}}{\Delta z} + (1-\beta)G_P + (1-\beta)G_B - \beta G_D - m_D D + m_P P$$

$$\frac{dN}{dt} = -\frac{J_{N.i+1} - J_{N.i}}{\Delta z} - JQ_1P$$
$$\frac{dA}{dt} = -\frac{J_{A.i+1} - J_{A.i}}{\Delta z} - JQ_2P - U_2 + \mu_B B + Z\left(\varepsilon\mu_Z + m_Z(1-\Omega)\right)$$
$$\frac{dDON}{dt} = -\frac{J_{DON.i+1} - J_{DON.i}}{\Delta z} + \gamma\sigma P + m_D D + (1-\varepsilon)\mu_Z Z - U_1$$

In addition, after the discretization, the damping of the light at a specific depth was approximated as follows:

$$damp = k_c dz\left(\sum_{j=1}^{i-1} P_j + \frac{P_i}{2} + \sum_{j=1}^{i-1} D_j + \frac{D_i}{2}\right)$$

In this case, the phytoplankton and detritus concentrations at all grid cells above the grid cell of interest *i* are summed. The summands $\frac{P_j}{2}$ and $\frac{D_j}{2}$ are added to account for that fact that the values calculated for each cell are assumed to be at the center of the cell and must therefore be corrected for the phytoplankton and detritus concentrations present in the upper half of the grid cell of interest *i*.

Diffusive and advective fluxes

Since the water column was divided into discrete grid cells, the advective and diffusive fluxes were calculated at the boundary between any two grid cells. The total flux of either of the 7 state variable at the boundary between two cells, *i* and *i+1*, is given by the sum of the advective (J_A) and diffusive (J_D) fluxes. The diffusive flux depends on the gradient of the concentration of any of the 7 state variables and has a direction following the gradient. This flux can be approximated by multiplying the difference in the concentrations of the two grid cells by a diffusivity coefficient, D_v, and dividing the result by Δz:

$$J_{d.i} = -D_v \frac{\phi_i - \phi_{i-1}}{\Delta z}$$

, where ϕ can be *P*, *Z*, *B*, *D*, *DON*, *A*, or *N* and D_v is the diffusivity coefficient.

The advective fluxes transport particulate matter downwards depending on its sinking velocity, *u*. In our model, only detritus and phytoplankton are affected by this flux. Zooplankton is motile enough for gravitational sinking to be negligible and all other state variables are only affected by diffusion. The advective fluxes of phytoplankton and detritus

are given by their specific sinking velocity, u_D and u_P, and the concentration of matter in the previous upstream cell:

$$J_{AP.i} = u_P P_{i-1}$$
$$J_{AD.i} = u_D D_{i-1}$$

Boundary conditions

As illustrated in figure 1 there are no fluxes between the atmosphere and the ocean, so:

$$J_{P,1} = J_{Z,1} = J_{B,1} = J_{A,1} = J_{DON,1} = J_{N,1} = J_{D,1} = 0$$

At the bottom of the water column there is a nitrate equilibrium between the sediment and the water effectively acting as either a source or sink of nutrients in our system:

$$J_{N,37} = -D_v \frac{N_b - N_{36}}{\Delta z_{36}}$$

The negative sign ensures that the transport of nitrate follows the gradient, so $-J_{N,37}$ gives an influx to the system in the differential equation of nitrate if $N_{36} < N_b$.
The other sink in our system is detritus being sequestered into the sediment, given by:

$$J_{D,37} = u_D \, D_{36}$$

The bottom fluxes of the rest of the state variables are given by:

$$J_{P,37} = J_{Z,37} = J_{B,37} = J_{A,37} = J_{DON,37} = 0$$

Parameters

The parameters for this study (see Table 1) are largely based on Fasham et al. (1990), but adjusted to an Arctic ecosystem by inferring values from other studies. In some cases, where it was not possible to find an exact parameter value, we used Fasham et al.'s, but adjusted it qualitatively, e.g., excretion by both zooplankton and detritus which decrease at higher latitudes (Alcaraz et al., 2012). The only instance where we use a parameter that we do not consider environmentally realistic is for the diffusivity. Here we took the highest estimate by Zhang et al., 2006 (10.8 m^2 d^{-1}) and multiplied it by two to be able to sustain a zooplankton population. As mentioned under "Conceptual model" the reason why we had to do this could be the lack of a stratified layer.

Table 1: Parameter values for our model.

Symbol	Description	Value	Unit	Reference
D_v	Diffusivity	21.6	$m^2\ d^{-1}$	Modified from Zhang et al., 2006
PAR_0	PAR/Total Irradiance	0.41	Fraction	Fasham et al., 1990
I_0	Annual average surface irradiance	200	$W\ m^{-2}$	Modified from Lu et al., 2018
k_w	Light attenuation due to water	0.04	m^{-1}	Fasham et al., 1990
g_P	Maximum growth rate of phytoplankton	2	d^{-1}	Modified from Fasham et al., 1990
α	Initial slope of P-I curve	0.025	$m^2\ W^{-1}\ d^{-1}$	Fasham et al., 1990
H_P	Half saturation for phytoplankton nutrient uptake	0.5	$mmol\ N\ m^{-3}$	Palmer et al., 2014
m_P	Phytoplankton specific mortality	0.1	d^{-1}	Palmer et al., 2014
k_c	Light attenuation due to phytoplankton and detritus	0.03	$m^2\ (mmol\ N)^{-1}$	Fasham et al., 1990
γ	Phytoplankton exudation fraction	0.03	Fraction	Billen et al., 1991
ψ	Ammonium inhibition for phytoplankton	1.5	$(mmol\ N)^{-1}$	Fasham et al., 1990
g_Z	Maximum growth rate of zooplankton	1.5	d^{-1}	Le Quéré et al., 2015
β	Zooplankton assimilation efficiency	0.75	Fraction	Fasham et al., 1990
μ_Z	Zooplankton specific excretion rate	0.025	d^{-1}	Modified from Fasham et al., 1990 and Alcaraz et al., 2012
m_Z	Zooplankton specific mortality rate	0.04	d^{-1}	Modified from Fasham et al., 1990 and Hirst et al., 2002
H_Z	Half saturation for zooplankton ingestion	1	$mmol\ N\ m^{-3}$	Fasham et al., 1990
Ω	Detrital fraction of zooplankton mortality	0.33	Fraction	Fasham et al., 1990
ε	Ammonium fraction of excretion by zooplankton	0.75	Fraction	Fasham et al., 1990
g_B	Maximum growth rate of bacteria	2	d^{-1}	Fasham et al., 1990
μ_B	Bacteria specific excretion rate	0.0125	d^{-1}	Modified from Fasham et al., 1990 and Alcaraz et al., 2012
H_B	Half saturation for bacterial nutrient uptake	0.1	$(mmol\ N)\ m^{-3}$	Le Fouest et al., 2015

η	Ammonium/DON uptake ratio for bacteria	0.6	Fraction	Fasham et al., 1990
m_D	Breakdown rate of detritus	0.05	d^{-1}	Le Fouest et al., 2015
u_D	Sinking rate of detritus	10	m d^{-1}	Modified from Le Fouest et al., 2015 and Fasham et al., 1990
u_P	Sinking rate of phytoplankton	1	m d^{-1}	Modified from Le Fouest et al., 2015 and Walsby et al., 2006
Δz	Size of grid cells	10, 50	m	
z	Water column depth	1000	m	
n	Number of grid cells	36	#	
θ	Latitude	70	° North	
p_P	Zooplankton preference for phytoplankton	0.7	Fraction	
p_B	Zooplankton preference for bacteria	0.1	Fraction	
p_D	Zooplankton preference for detritus	0.2	Fraction	
N_b	Nitrate concentration in the sediment	15	(mmol N) m^{-3}	Ocean Data view, 2023
W_{center}	Middle of ice coverage	60	Julian day	
W_{length}	Length of ice coverage	60, 120, 180	d	

Results and discussion

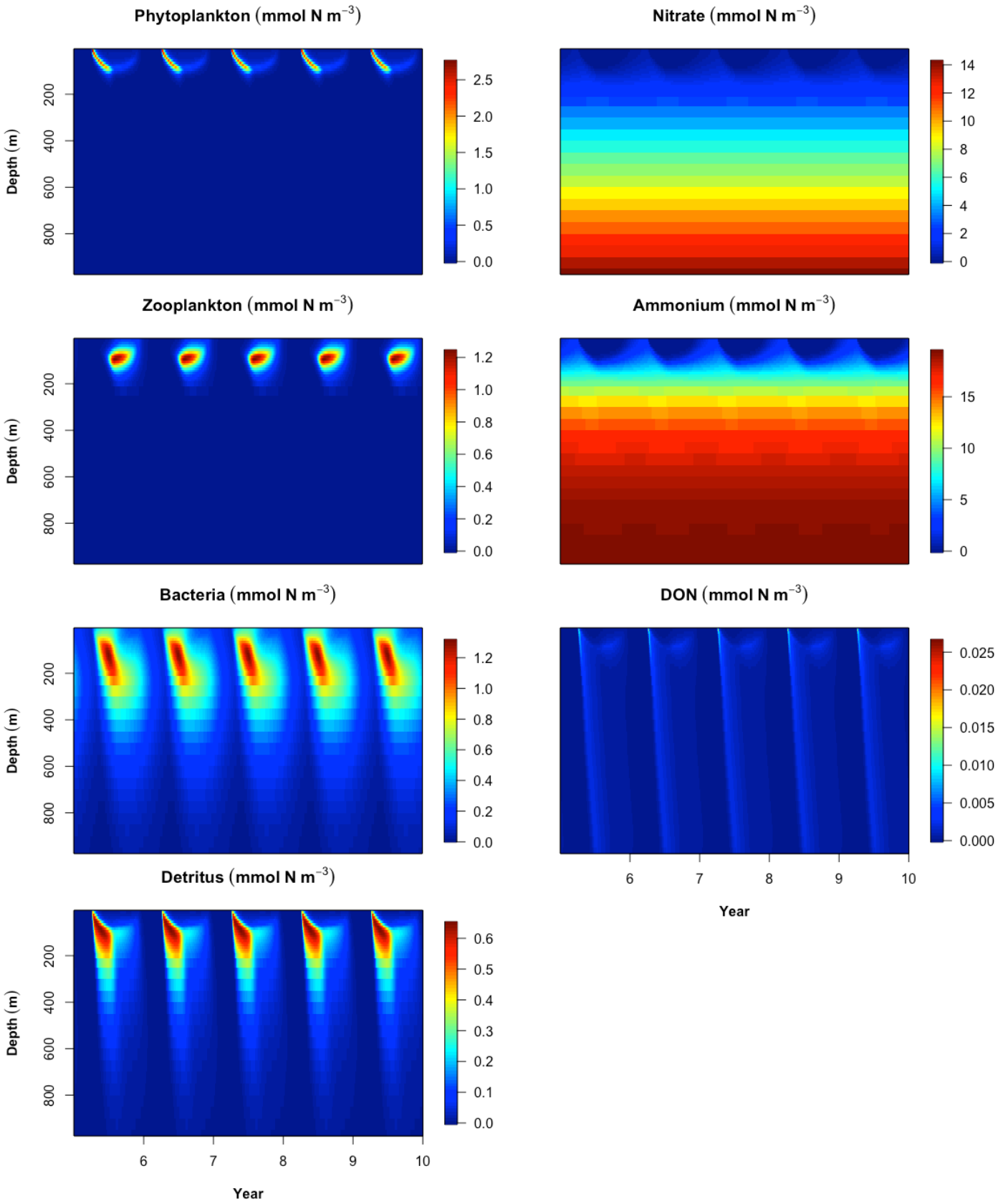

Figure 6: Image plot for the seven state variables, i.e., phytoplankton, zooplankton, bacteria, detritus, nitrate, ammonium, and DON based on the converged solution. The plots are based on the 6 months ice scenario i.e., the baseline of the system.

Figure 6 shows seven image plots, one for each of the state variables based on the converged solution. The seasonality of the system can clearly be seen from the repetitive patterns. When the ice breaks in the late spring the phytoplankton starts to form a bloom in the surface. Subsequently, nitrate and ammonium are depleted in the surface water following the trend of phytoplankton. The phytoplankton bloom progresses further down in the water column as the nutrients are being depleted. Below the productive layer, the concentration of ammonium increases faster with depth than the concentration of nitrate. The reason for this is that ammonium is created throughout the whole water column by the excretion of zooplankton and bacteria, whereas nitrate is only supplied from the sediment. Following a bloom of phytoplankton, the presence of zooplankton increases. Phytoplankton and zooplankton promote the production of detritus, which can be observed as well. DON is produced from zooplankton, phytoplankton, and detritus, and together with ammonium that can sustain the production of bacteria throughout almost the whole year. Since nitrification, i.e., the process whereby ammonium is converted into nitrate, is not included in our ecosystem, there is a buildup of ammonium near the bottom, which can be seen in the image plot.

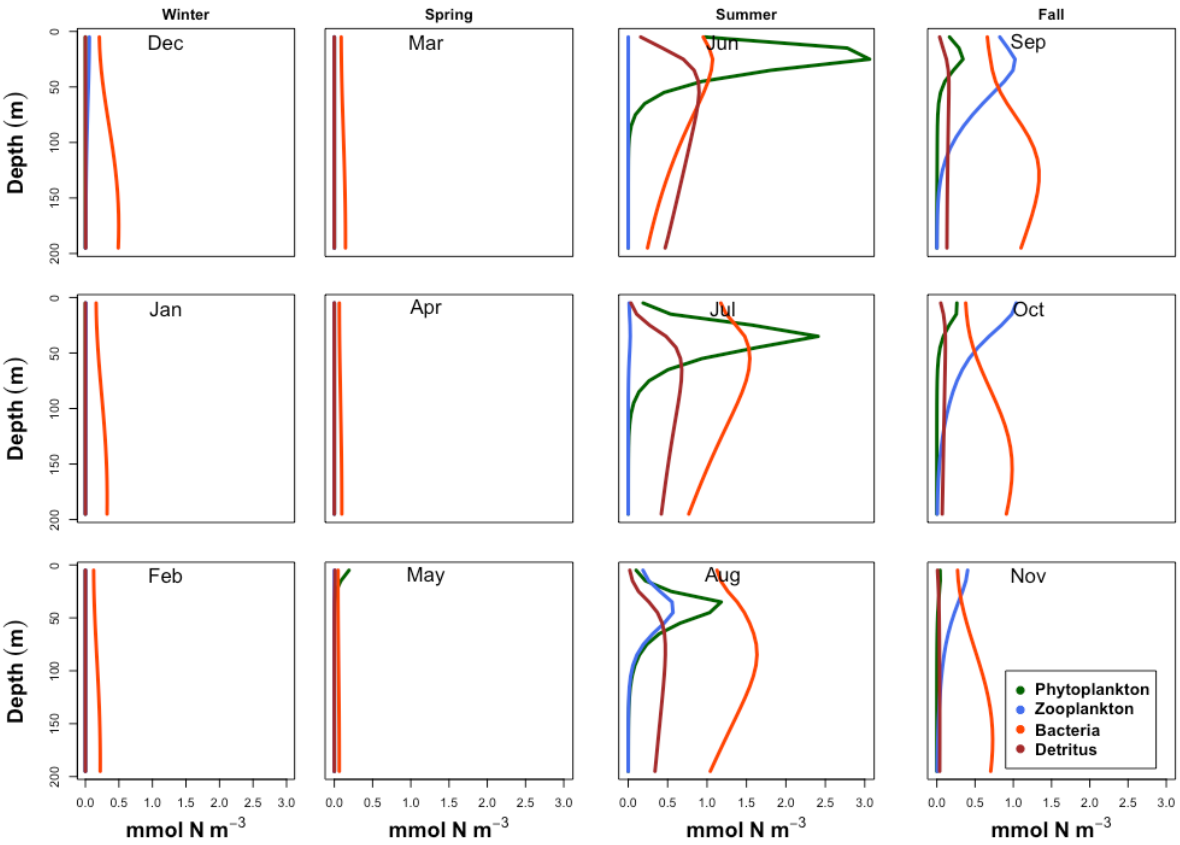

Figure 7: Vertical profiles for the particulate constituents of the system, i.e., phytoplankton, zooplankton, bacteria, and detritus. The profiles are made after the solution has converged (110 years), and each plot represents day 15 in each of the months. The plots are based on the 6 months ice scenario i.e., the baseline of the system.

From Figure 7 vertical profiles of the particulate constituents can be seen. During winter a low concentration of bacteria has been able to sustain themselves from the previous fall production of DON and ammonium, whereas none of the other particulate constituents are present. During spring there is practically no concentration of either of the four particulate constituents. When the ice starts to break up during late spring, the spring bloom is initiated, which can be seen on the June plot. June is characterized by a large bloom of phytoplankton as well as bacteria and detritus. In the following months, the concentration of the chlorophyll maximum and the detritus decreases until November, where the concentration approaches zero. A relatively high concentration of zooplankton establishes during August as sufficient food is present. The zooplankton concentration is able to sustain itself until early December, where most of it disappears. The concentration of bacteria increases during summer followed by a slow decrease during fall and winter, where it eventually approaches zero. The presence of bacteria during fall and winter is likely supported by the concentration of detritus.

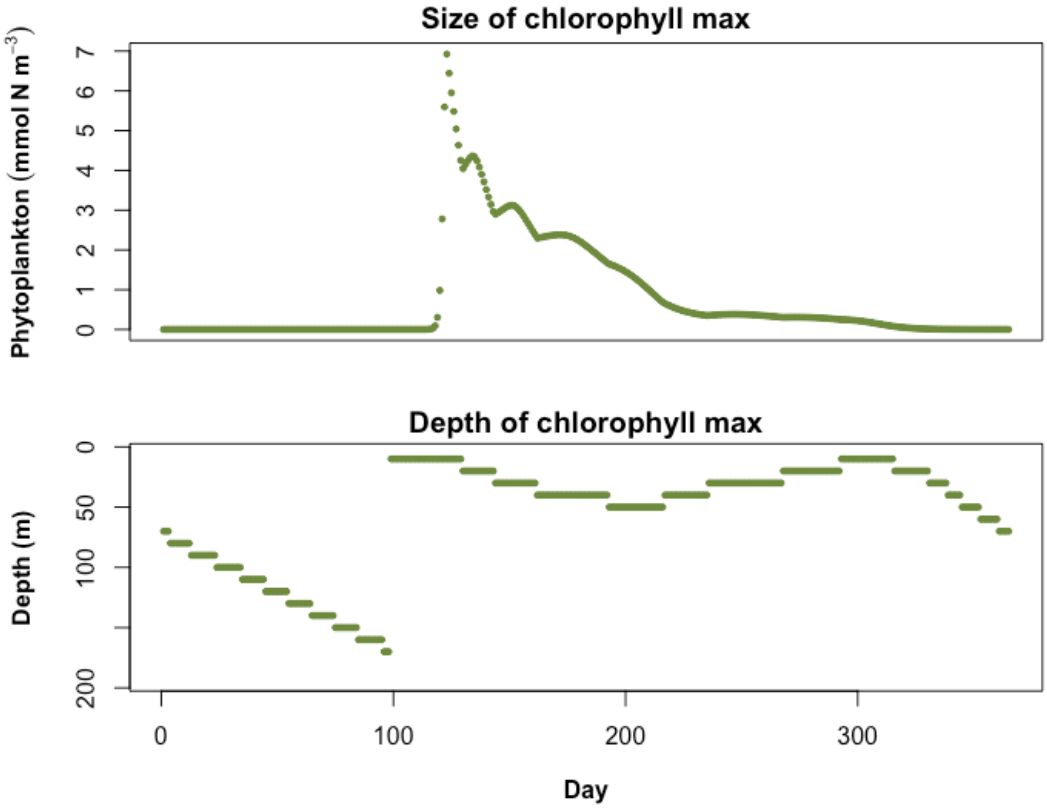

Figure 8: The evolution of the concentration and the depth of the chlorophyll maximum throughout a year, after the solution has converged (110 years). The plots are based on the 6 months ice scenario i.e., the baseline of the system.

Figure 8 shows the evolution of the concentration and the depth of the chlorophyll maximum throughout a year. Initially, the concentration of the chlorophyll maximum is close to zero, as the ice cover inhibits the phytoplankton growth. In that same period, the small amount of phytoplankton present in the water column slowly sinks. In the late spring when the ice breaks up, the concentration of the chlorophyll maximum increases rapidly due to the initiation of the surface spring bloom. This can be seen from the shallow depth of chlorophyll maximum. The concentration of chlorophyll then decreases, and the maximum becomes deeper. During the fall, the depth of the maximum increases slightly, likely due to the grazing by zooplankton. Eventually, during winter the concentration of the chlorophyll maximum approaches zero again and the depth of the maximums becomes greater again.

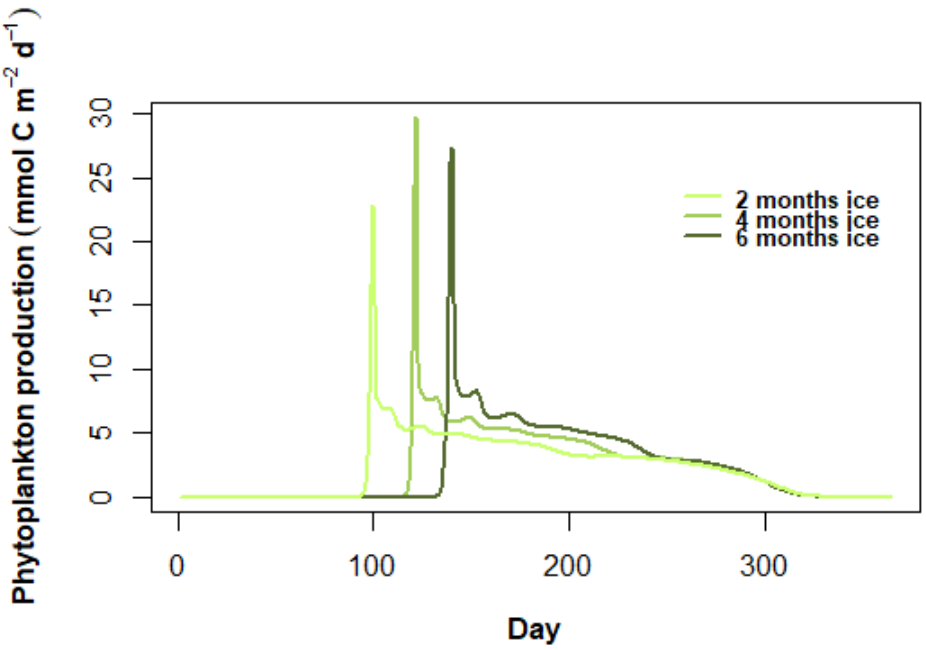

Figure 9: Evolution of phytoplankton production during a year (converged after 110 years), under the three different ice cover scenarios

From Figure 9 it can be seen that the phytoplankton production throughout the year depends on the ice coverage. A short period of ice results in an earlier phytoplankton bloom and a lower maximum production. A long period of ice results in a later phytoplankton bloom, however, not a higher maximum production. According to Table 2 the annual production of phytoplankton is lowest in the two month ice scenario, and highest in the four month scenario. This is counterintuitive, as one would think that a shorter period of ice would result in an overall higher production. Likely, this is due to the fact that a longer ice duration promotes a more intense bloom compared to a shorter duration of ice, and therefore the

overall production is fairly constant. However, it seems that the optimal ice cover for primary production is of intermediate duration.

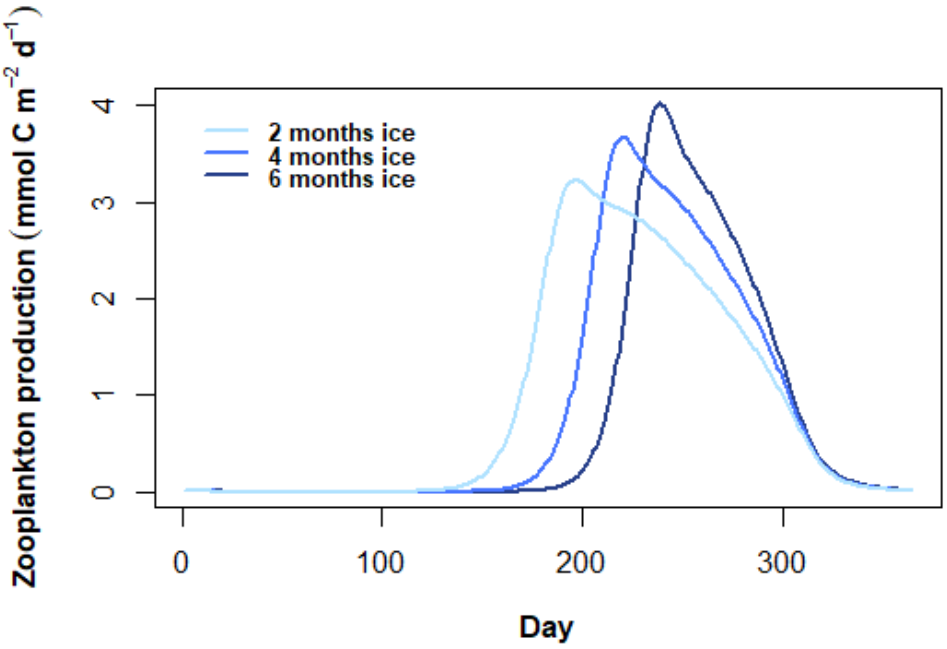

Figure 10: Evolution of zooplankton production during a year (converged after 110 years), under the three different ice cover scenarios.

From Figure 10 it can be seen that the zooplankton production is dependent on the sea ice coverage. On one hand, it can be seen that the shorter period with ice, the lower the maximum production and the sooner the peak of the production happens. On the other hand, shorter period of ice results in a higher annual production of zooplankton, which can also be seen from Table 2. The zooplankton supports the higher trophic levels including commercially exploited fish species. Therefore, given the higher annual production of zooplankton, one would believe that the fisheries would be able to harvest more biomass in the future. However, the transfer of energy to the higher trophic levels is sensitive to the phenology of the spring bloom and its grazers, which should be kept in mind while interpreting the results.

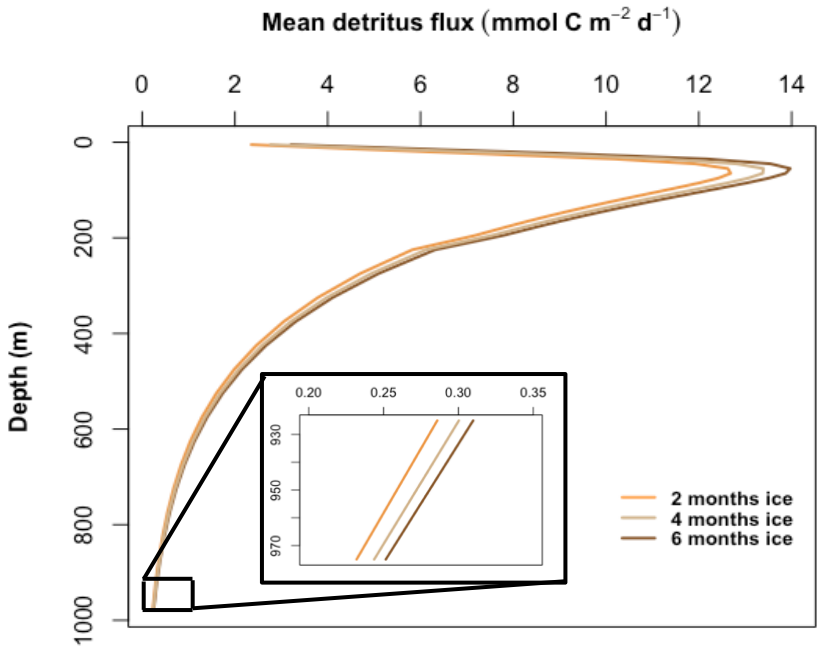

Figure 11: Flux of detritus as a function of depth under the three different ice coverage scenarios, the solution is converged (after 110 years). The values are mean values of a whole year.

Figure 11 shows the annual mean detritus flux throughout the water column, which is also known as a Martin curve. It can be seen that the largest flux is found approximately 100 meter down in the water column corresponding to just below the production peak, and that the flux near the bottom is only a fraction of the flux higher up in the water column. The declining trend of the curve depend on zooplankton feeding and biodegradation of detritus throughout the water column. Long periods of ice results in a consistently higher flux, likely due to the intense phytoplankton bloom upon breaking of the ice.

Table 2: Maximum and annual production of phytoplankton and zooplankton as well as the carbon export under the three different ice coverage scenarios.

	Phytoplankton		**Zooplankton**		**Carbon**
	Maximum production (mmol C m^{-2} d^{-1})	Annual production (mmol C m^{-2})	Maximum production (mmol C m^{-2} d^{-1})	Annual production (mmol C m^{-2})	Annual sequestration (mmol C m^{-2})
Scenario 6	27.3	813.7	4.0	266.8	91.8
Scenario 4	29.7	818.5	3.7	299.5	88.9
Scenario 2	22.9	816.5	3.2	331.6	84.7

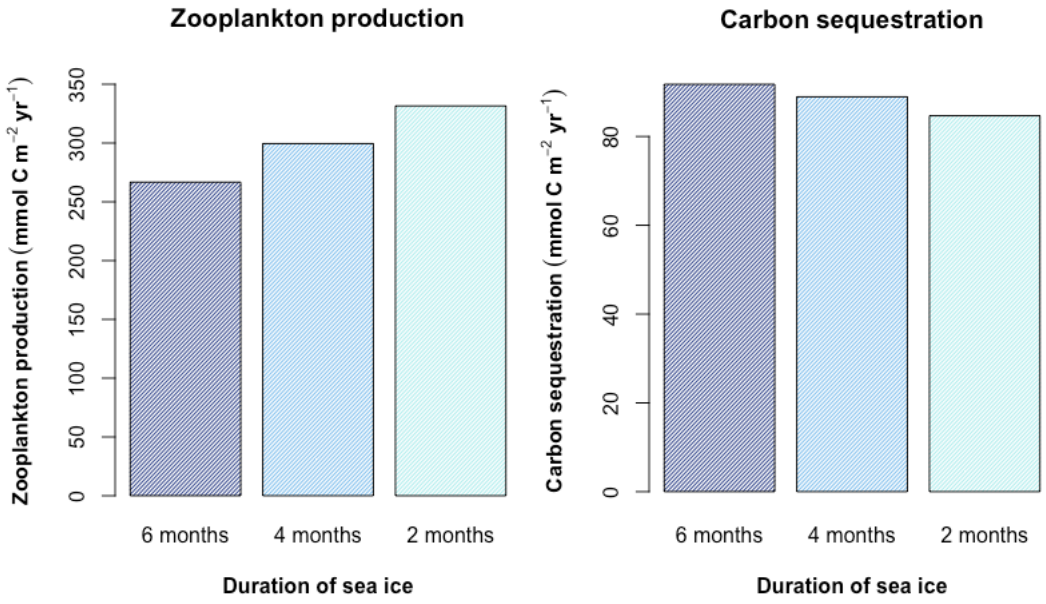

Figure 12: Bar plots showing the annual zooplankton production and carbon sequestration under the three scenarios of ice coverage.

Figure 12 shows the annual zooplankton production and carbon sequestration during all scenarios. The annual zooplankton production is increasing with decreasing duration of ice by 12.3% and 24.3% for four and two months scenarios, respectively. The annual carbon sequestration is decreasing with decreasing duration of ice by 3.1% and 7.7% for scenario four and two months, respectively. The reason for this is likely that a longer period of ice coverage, results in a more rapid phytoplankton bloom once the ice breaks up and thus a more intense flux of carbon through the water column. Therefore, the ecosystem services might change in the future with fisheries expected to increase and carbon sequestration expected to decrease.

Sensitivity analysis

As we have a lot of parameters a full sensitivity analysis for all of them was not possible. However, we chose to investigate the sensitivity of diffusivity, as this was a parameter we suspect to be environmentally unrealistic. Figure XX shows the vertical distribution of phytoplankton in mid-august after we ran the model for 100 years. Here it can be seen that both magnitude and depth of chlorophyll max increases with increasing diffusivity. The only exception is the highest diffusivity, which has a smaller chlorophyll max, but this could just be due to the solution not being converged. However, due to computational time, it was impossible to run it for a longer period.

Overall, it seems that diffusivity is very important in controlling primary production and

thereby the energy for the whole food web, and for further investigations using our model, energy should be put into giving this parameter environmental relevance.

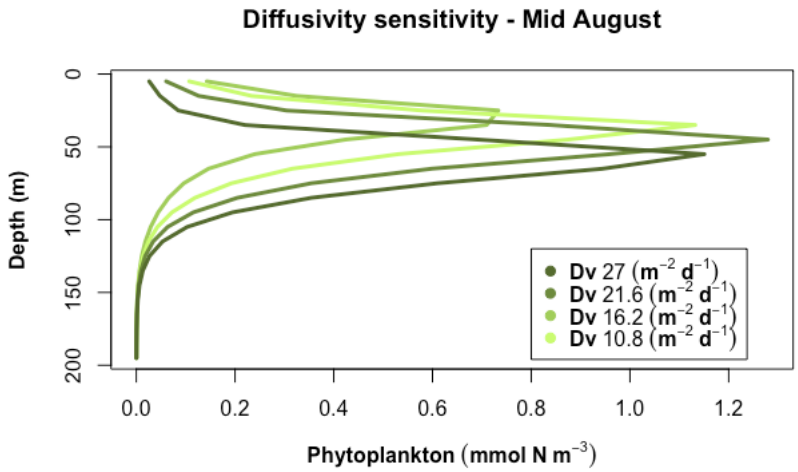

Figure 13: Phytoplankton concentration throughout the water column in mid-August after the solution has converged (100 years) for varying values of diffusivity.

Conclusion

The aim of this project was to investigate carbon sequestration in the Arctic under different scenarios of sea ice durations. We found that a decrease in sea ice duration from six to four months, and from six to two months, would cause a decrease in carbon sequestration of 3.1% and 7.7%, respectively. Since carbon sequestration is one of the main ecosystem services, the shortening of the ice period could have negative implications for future climate. Furthermore, going from sea ice duration of six to four months, and from six to two months, resulted in an increase in annual zooplankton production by 12.3% and 24.3%, respectively. The increase in zooplankton production could lead to an increased transfer of energy to higher trophic levels. Fisheries are another main ecosystem service, and it is expected to be positively affected by the decrease in sea ice. On the other hand, phenology of the spring bloom is projected to change as well, which could impact the link between zooplankton and fish production negatively.

GitHub

https://github.com/EmilBohr/Fasham_model.git

References

Alcaraz, M., Almeda, R., Saiz, E., Calbet, A., Duarte, C.M., Agustí, S., Santiago, R. and Alonso, A. (2012). Temperature dependence of Arctic zooplankton metabolism and excretion stoichiometry. *Biogeosciences Discussions*, 9(6), pp.7443–7463. doi:https://doi.org/10.5194/bgd-9-7443-2012.

Anderson, L.A., and Sarmiento, J.L. (1994). Redfield ratios of remineralization determined by nutrient data analysis. *Global Biogeochemical Cycles*, 8(1), pp.65–80. doi:https://doi.org/10.1029/93gb03318.

Behrenfeld, M.J. (2010). Abandoning Sverdrup's Critical Depth Hypothesis on phytoplankton blooms. *Ecology*, 91(4), pp.977–989. doi:https://doi.org/10.1890/09-1207.1.

Billen, G. and Becquevort, S. (1991). Phytoplankton-bacteria relationship in the Antarctic marine ecosystem. *Polar Research*, 10(1), pp.245–254. doi:https://doi.org/10.1111/j.1751-8369.1991.tb00650.x.

Box, J.E., Colgan, W.T., Christensen, T.R., Schmidt, N.M., Lund, M., Parmentier, F.-J.W., Brown, R., Bhatt, U.S., Euskirchen, E.S., Romanovsky, V.E., Walsh, J.E., Overland, J.E., Wang, M., Corell, R.W., Meier, W.N., Wouters, B., Mernild, S., Mård, J., Pawlak, J. and Olsen, M.S. (2019). Key indicators of Arctic climate change: 1971–2017. *Environmental Research Letters*, 14(4), p.045010. doi:https://doi.org/10.1088/1748-9326/aafc1b.

Corinne Le Quéré, Buitenhuis, E.T., Moriarty, R., Séverine Alvain, Olivier Aumont, Bopp, L., Chollet, S., Enright, C., Franklin, D.J., Geider, R.J., Harrison, S.P., Hirst, A., Larsen, S., Legendre, L., Platt, T., Iain Colin Prentice, Rivkin, R.B., Shubha Sathyendranath, Stephens, N. and Vogt, M. (2015). Role of zooplankton dynamics for Southern Ocean phytoplankton biomass and global biogeochemical cycles. *Biogeosciences Discussions*. doi:https://doi.org/10.5194/bgd-12-11935-2015.

Fasham, M.J.R., Ducklow, H.W. and McKelvie, S.M. (1990). A nitrogen-based model of plankton dynamics in the oceanic mixed layer. *Journal of Marine Research*, 48(3), pp.591–639. doi:https://doi.org/10.1357/002224090784984678.

Francis, J.A. and Wu, B. (2020). Why has no new record-minimum Arctic sea-ice extent occurred since September 2012? *Environmental Research Letters*, 15(11), p.114034. doi:https://doi.org/10.1088/1748-9326/abc047.

Hirst, A. and Kiørboe, T. (2002). Mortality of marine planktonic copepods: global rates and patterns. *Marine Ecology Progress Series*, 230, pp.195–209. doi:https://doi.org/10.3354/meps230195.

Im, U., Tsigaridis, K., Faluvegi, G., Langen, P.L., French, J.P., Mahmood, R., Thomas, M.A., von Salzen, K., Thomas, D.C., Whaley, C.H., Klimont, Z., Skov, H. and Brandt, J. (2021). Present and future aerosol impacts on Arctic climate change in the GISS-E2.1 Earth system model. *Atmospheric Chemistry and Physics*, 21(13), pp.10413–10438. doi:https://doi.org/10.5194/acp-21-10413-2021.

Jahn, A. (2018). Reduced probability of ice-free summers for 1.5 °C compared to 2 °C warming. *Nature Climate Change*, 8(5), pp.409–413. doi:https://doi.org/10.1038/s41558-018-0127-8.

Lannuzel, D., Tedesco, L., van Leeuwe, M., Campbell, K., Flores, H., Delille, B., Miller, L., Stefels, J., Assmy, P., Bowman, J., Brown, K., Castellani, G., Chierici, M., Crabeck, O., Damm, E., Else, B., Fransson, A., Fripiat, F., Geilfus, N.-X. and Jacques, C. (2020). The future of Arctic sea-ice biogeochemistry and ice-associated ecosystems. *Nature Climate Change*, 10(11), pp.983–992. doi:https://doi.org/10.1038/s41558-020-00940-4.

Le Fouest, V., Manizza, M., Tremblay, B. and Babin, M. (2015). Modelling the impact of riverine DON removal by marine bacterioplankton on primary production in the Arctic Ocean. *Biogeosciences*, 12(11), pp.3385–3402. doi:https://doi.org/10.5194/bg-12-3385-2015.

Lu, P., Cheng, B., Leppäranta, M. and Li, Z. (2018). Partitioning of solar radiation in Arctic sea ice during melt season. *Oceanologia*, 60(4), pp.464–477. doi:https://doi.org/10.1016/j.oceano.2018.03.002.

Masson-Delmotte, V.P., Zhai, A., Pirani, S.L., Connors, C., Péan, S., Berger, N. Caud, Y. Chen, L. Goldfarb, M.I., Gomis, M., Huang, K., Leitzell, E., Lonnoy, J.B.R., Matthews, T.K., Maycock, T,. Waterfield, O., Yelekçi, R., Yu and B. Zhou (eds.) (2021). 'IPCC, 2021: Summary for Policymakers. In: Climate Change 2021: The Physical Science Basis.

Contribution of Working Group I to the Sixth Assessment Report of the Intergovernmental Panel on Climate Change'. Cambridge University Press. *In Press*, www.ipcc.ch/report/ar6/wg1/downloads/report/IPCC_AR6_WGI_SPM.pdf

Palmer, M.A., Saenz, B. and Arrigo, K.R. (2014). Impacts of sea ice retreat, thinning, and melt-pond proliferation on the summer phytoplankton bloom in the Chukchi Sea, Arctic Ocean. *Deep Sea Research Part II: Topical Studies in Oceanography*, 105, pp.85–104. doi:https://doi.org/10.1016/j.dsr2.2014.03.016.

Smith, D.M., Screen, J.A., Deser, C., Cohen, J., Fyfe, J.C., García-Serrano, J., Jung, T., Kattsov, V., Matei, D., Msadek, R., Peings, Y., Sigmond, M., Ukita, J., Yoon, J.-H. and Zhang, X. (2019). The Polar Amplification Model Intercomparison Project (PAMIP) contribution to CMIP6: investigating the causes and consequences of polar amplification. *Geoscientific Model Development*, 12(3), pp.1139–1164. doi:https://doi.org/10.5194/gmd-12-1139-2019.

Sverdrup, H.U. (1953). On Conditions for the Vernal Blooming of Phytoplankton. *ICES Journal of Marine Science*, 18(3), pp.287–295. doi:https://doi.org/10.1093/icesjms/18.3.287.

Walsby, A.E. and Daryl Philip Holland (2006). Sinking velocities of phytoplankton measured on a stable density gradient by laser scanning. The Royal Society Publishing, 3(8), pp.429–439. doi: https://doi.org/10.1098/rsif.2005.0106.

Zhang, J. and Steele, M. (2007). Effect of vertical mixing on the Atlantic Water layer circulation in the Arctic Ocean. *Journal of Geophysical Research*, 112(C4). doi:https://doi.org/10.1029/2006jc003732.